RSC Sustainability

ROYAL SOCIETY OF CHEMISTRY

PAPER

View Article Online
View Journal | View Issue

Cite this: *RSC Sustainability*, 2024, **2**, 635

One-pot synthesis of carbon dots from neem resin and the selective detection of Fe(II) ions and photocatalytic degradation of toxic dyes†

S. Gokul Eswaran,[ab] T. Stalin,[c] D. Thiruppathi,[d] Manivannan Madhu,[a] S. Santhoshkumar,[a] Jolanta Warchol,[f] A. Santhana Krishna Kumar,*[a] Wei-Lung Tseng*[ae] and N. Vasimalai*[b]

The sustainable utilization of biomass has attracted great interest worldwide. A remarkably brand-new, environmentally friendly technique is created to prepare fluorescent carbon dots (CDs). This study used neem resin as a hydrothermal precursor to synthesize neem resin-derived CDs (NR-CDs). Electron microscopy- and spectroscopy-related techniques were used to characterize these NR-CDs. These NR-CDs exhibited a fluorescence peak at 420 nm with a quantum yield of 21%, allowing them for sensitive detection of Fe^{2+} ions with a corresponding limit of detection as low as 14 nM. The as-synthesised NR-CD fluorescent probe was applied to determine Fe^{2+} in real samples of drinking, river, and tap water, highlighting its practical applications. Additionally, these NR-CDs were utilized as a photocatalyst to degrade Rhodamine B, Fast Green, and Naphthol Yellow dyes in industrial wastewater in the presence of $NaBH_4$ as a surface defect modifier. Under exposure to visible light, NR-CDs were highly efficient for degrading Rhodamine B, Fast Green, and Naphthol Yellow, with degradation rates of 93.13%, 93.01%, and 91.29%, respectively. The proposed mechanism outlines a multi-step process for photocatalytic degradation of organic dyes by using the NR-CDs; further this study demonstrates the multifaceted utility of NR-RCDs in diverse applications, from ion detection in environmental samples to bio-imaging and efficient catalytic degradation of various dyes.

Received 4th November 2023
Accepted 26th January 2024

DOI: 10.1039/d3su00404j

rsc.li/rscsus

Sustainability spotlight

The apprehension over emerging ground water pollution by aromatic organic dyes from industries has evoked increasing concerns for public health due to their toxicity and carcinogenicity. Hence, it's vital to treat polluted wastewater before its discharge. Using nano-materials has emerged as a viable alternative approach to tackle this problem. Neem resin-derived CDs (NR-CDs) were utilized as a photo-catalyst to degrade Rhodamine B, Fast Green, and Naphthol Yellow dyes in industrial wastewater in the presence of $NaBH_4$, serving as a promising candidate in environmental remediation because of their high catalytic efficiency. This study aims to highlight an environmentally benign approach for degradation of organic dyes, which certainly paves a way to remediate various other emerging pollutants from wastewater streams. The as-synthesized NR-CDs exhibit a fluorescence peak at 420 nm with a quantum yield of 21%, allowing them for the sensitive detection of Fe^{2+} ions with a corresponding limit of detection as low as 14 nM. Subsequently, the as-synthesized neem resin-derived CD (NR-CD) fluorescent probe was employed to determine Fe^{2+} in real samples of drinking, river, and tap water, highlighting its practical application.

1. Introduction

Neem, scientifically known as *Azadirachta indica*, is a versatile plant widely recognized for its numerous medicinal and therapeutic properties.[1] Neem contains various chemicals, such as gallic acid, saponins, limonoids, catechins, quercetins, anthocyanins, tannins, flavonoids, and other minor polyphenols. The presence of these components in neem makes its

[a]*Department of Chemistry, National Sun Yat-Sen University, No. 70, Lien-hai Road, Gushan District, Kaohsiung, 80424, Taiwan. E-mail: tsengwl@mail.nsysu.edu.tw*

[b]*Department of Chemistry, B.S. Abdur Rahman Crescent Institute of Science and Technology, Vandalur, Chennai 600 048, India*

[c]*Department of Industrial Chemistry, Alagappa University, Karaikudi 630 003, Tamil Nadu, India*

[d]*Department of Chemistry, Vivekananda College, Tiruvedakam West, Madurai, 625 234, India*

[e]*School of Pharmacy, Kaohsiung Medical University, No. 100, Shiquan 1st Road, Sanmin District, Kaohsiung City 80708, Taiwan*

[f]*Department of Advanced Material Technology, Faculty of Chemistry, Wroclaw University of Science and Technology, ul. M. Smoluchowskiego 25, Wroclaw City 50-372, Poland*

† Electronic supplementary information (ESI) available: Detailed information related to the fluorescence intensity of the proposed probe (NR-CDs) for stability studies and also, emission intensity against various concentrations of NaCl (ionic strength); the pH study against fluorescence emission intensity with different pHs (Fig. S1). UV-vis DRS spectra for the presence of the NR-CD nano-catalyst for the Tauc plot and EPR spectra for irradiation of visible light (Fig. S2). Fluorescence spectroscopy study for monitoring the reaction of terephthalic acid (Fig. S3). See DOI: https://doi.org/10.1039/d3su00404j

related products biocompatible and safe for use in various applications such as biomedicine, food, and personal care products. This is supported by the fact that neem resin is still used for many commercial items, including toothpaste, soap, cosmetics, and insect repellents. Additionally, neem is still used to cure gastrointestinal ailments, leprosy, jaundice, rheumatism, chickenpox, fever, and headaches. Besides its extensive use in traditional medicine, neem has also gained significant attention in nanotechnology. This remarkable plant is a valuable source for synthesizing various nanoparticles.[1] Nanoparticles, with 1–100 nanometer dimensions, have unique physical and chemical properties that make them highly desirable in various scientific and technological applications.[2] Neem extracts, such as neem leaf, neem seed, and neem bark, contain a wide array of bioactive compounds with inherent capabilities to act as reducing agents, stabilizing agents, and capping agents in nanoparticle synthesis.[3] One of the most common nanoparticles synthesized using neem is silver nanoparticles.[4,5] Neem extracts, particularly neem leaf extract, effectively reduce silver ions to silver nanoparticles.[6] The phytochemicals present in neem, such as flavonoids, terpenoids, and phenolic compounds, are responsible for the reduction process and stabilizing the resulting silver nanoparticles.[7,8] Apart from silver nanoparticles, neem has also been utilized in synthesizing other nanoparticles, including gold,[9] zinc oxide,[10] titanium dioxide,[11] zero-valent iron,[12] magnesium oxide,[13] iron oxide,[14] silicon oxide,[15] and copper.[16] The unique composition of neem extracts allows successful reduction and stabilization of these nanoparticles, making neem an attractive and eco-friendly alternative to conventional chemicals. The synthesis of nanoparticles using neem offers several advantages. First, neem is readily available in many parts of the world, making it a cost-effective and sustainable source for nanoparticle synthesis. Second, the bioactive compounds in neem extracts exhibit inherent antimicrobial, antioxidant, and anti-inflammatory properties, which can be transferred to the synthesized nanoparticles, enhancing their potential applications in various fields, including medicine, agriculture, and environmental remediation. Lastly, neem is a renewable resource, and its extraction does not require toxic chemicals, making it an attractive choice for nanoparticle synthesis.

Carbon dots (CDs) are nanoscale carbon-based materials with unique optical and electronic properties.[17] CDs have several advantages in their optical properties, such as their broadened optical absorption, color-tunable emission, good fluorescence quantum yield, and good photobleaching resistance.[18] Owing to these remarkable features, they have garnered immense interest for their potential applications in areas such as bioimaging,[19] sensing,[20] electrochemical studies,[21] and energy storage. To maintain the excellent optical properties of CDs without reducing production costs, researchers have explored various methods for synthesizing CDs based on a variety of precursors, including organic compounds, agricultural waste, natural polymers,[22] and plant extracts.[23] Given the success of neem extract in synthesizing metal and metal oxide nanoparticles, it emerges as a promising precursor material for the preparation of CDs.[18] Organic compounds in neem extracts, featuring functional groups like hydroxyl (–OH), carbonyl (C=O), and carboxyl (–COOH), offer abundant opportunities for surface functionalization and tailoring the properties of CDs. In response to this intriguing hypothesis, we introduced a straightforward and simplified hydrothermal reaction process for neem resin-derived CDs (NR-CDs). The as-synthesized NR-CDs exhibited stable fluorescence with a maximum emission of 420 nm and quantum yield of 21% when excited at 330 nm, making them promising for lighting and display technology applications. The NR-CDs demonstrate good stability over six months, along with tolerance to ionic strength up to 50 mM and optimal fluorescence intensity at pH 7.2. The unique optical properties of NR-CDs, combined with their surface functionalization potential, make them excellent candidates for the sensitive and selective detection of Fe^{2+} ions. Additionally, the NR-CDs, with their photostable nature and excellent light-absorbing properties, are efficient photocatalysts for breaking down harmful organic pollutants in wastewater.

2. Experimental section

2.1. Chemicals

Ferric chloride, copper sulfate, sodium chloride, potassium chloride, zinc nitrate, magnesium chloride, lithium chloride, monosodium dihydrogen phosphate, Rhodamine B, Fast Green, di-sodium mono-hydrogen phosphate, Naphthol yellow, nickel sulfate, chromium sulfate, manganese chloride, and lead nitrate were received from Sigma-Aldrich. The dialysis tubes (29.3 mm diameter, 3.5 kDa (MW)) were purchased from Sigma-Aldrich. The pH buffer solution was created using monosodium dihydrogen phosphate and di-sodium mono-hydrogen phosphate. The pH was balanced by using NaOH and HCl. The entire experiment was carried out using Millipore water.

2.2. Synthesis of the NR-CDs and their characterization

Neem resin, sourced from our institute's campus, weighing 10 g, was blended with 100 mL of Millipore water and left to stand in a dark room. The resulting extract solution was filtered and subsequently used as a precursor for synthesizing the NR-CDs, which were synthesized using an eco-friendly approach. Initially, 0.5 g of neem resin was dissolved in 20 mL of distilled water, placed in a Teflon-coated autoclave, and heated to 180 °C for 8 hours. Following cooling to room temperature, the resulting solution underwent centrifugation at 4000 rpm for 10 min, followed by filtration through a 0.2 μm cellulose filter. The solution was then subjected to a two-day dialysis process, with changing Millipore water every 6 hours. The purified CDs denoted as NR-CDs were stored at 4 °C for future use. The fluorescence, absorption, and FT-IR spectra for NR-CDs were recorded on a JASCO FP-8200 spectrofluorometer (JASCO Corp., Tokyo, Japan) and PerkinElmer Lambda 25 UV-vis spectrophotometer (PerkinElmer, Lambda XLS, USA), respectively. The crystalline structure of NR-CDs was acquired by X-ray diffraction (XRD) (Bruker D8 Advance, Bruker, USA), followed by high-resolution transmission electron microscopy (HR-TEM) using a JEOL-2100 instrument (JEOL, Ltd Tokyo, Japan) operating at 200 kV.

2.3. Fluorescence detection of Fe^{2+} ions

The detection of Fe^{2+} ion concentration was conducted by applying the standard addition method as follows: different concentrations of Fe^{2+} ions, ranging from 4 to 71 μM, were individually prepared in separate 5 mL Eppendorf centrifuge vials containing a phosphate buffer solution (2.5 mL, 100 mM of PBS, pH 7.2). Subsequently, the centrifuge vials were incubated with an addition of 0.2 mL of NR-CDs with gentle shaking for 30 minutes at room temperature. Afterward, the resulting mixture was transferred to a quartz cuvette and then the emission spectra were measured by using a fixed excitation wavelength of 330 nm. A calibration curve was constructed by plotting the observed fluorescence changes against the concentrations of Fe^{2+} ions introduced into the cuvette. The limit of detection (LOD) for Fe^{2+} ions was determined based on a signal-to-noise ratio of 3; generally this can be calculated by using the $3\sigma/m$ formula, where "σ" is the standard deviation, "m" is the slope of the calibration graph and 3 is three times replication. The selectivity of NR-CDs was examined by replacing Fe^{2+} ions with other metal ions one at a time. In analysing real samples, river, drinking, and tap water samples were employed as the test subjects. To prepare these samples, the collected water underwent filtration using Whatman No. 1 filter paper, effectively removing dust particles. Subsequently, a known concentration of Fe^{2+} ions was spiked into the real sample solution. The resultant solution was incubated with the as-proposed NR-CD fluorescence probe at pH 7.2, followed by recording the corresponding fluorescence spectra.

2.4. Photocatalytic degradation of dyes

In 5 mL Eppendorf centrifuge vials, degradation studies were initiated by adding 2 mL of water and 100 μL of three different dyes (Naphthalene Yellow, Rhodamine B, and Fast Green). Subsequently, 200 μL of NR-CDs and 100 μL of sodium borohydride (0.1 mM) were sequentially added to the resulting solution, and visible light-mediated photo-catalytic degradation was performed by irradiation with a blue-emitting LED (KESSIL-PR160, Richmond, CA; λ_{max} of 456 nm, the optical power of 30 W) for 0 to 60 min at room temperature. We carefully observed the spectral changes every minute by using a UV-visible spectrophotometer. By monitoring the minute-by-minute spectral changes in the presence of NR-CDs, we could assess the degradation efficiency of these dyes. The obtained data allowed us to construct degradation kinetics profiles, providing insights into the rate and mechanisms of dye decomposition over time.

3. Results and discussion

3.1. Optical properties of NR-CDs and their characterization

The NR-CDs were synthesized following an environmentally friendly approach without using organic solvents. The formation mechanism of NR-CDs typically involves several stages. Initially, the organic molecules in neem resin extracts undergo self-assembly and condensation, forming small clusters or nuclei under the hydrothermal treatment. After nucleation, the nuclei grow and transform into carbon-rich structures through carbonization. During carbonization, the as-formed NR-CDs can develop surface defects and functional groups, such as hydroxyl (–OH), carbonyl (C=O), and carboxyl (–COOH) groups. These functional groups can contribute to the surface passivation and stabilization of the NR-CDs.

The as-synthesized NR-CDs were characterized through various analytical techniques, including absorption, fluorescence, FT-IR spectroscopy, XRD, and HR-TEM, to assess their optical and structural properties. The UV-vis spectrum of NR-CDs shows absorption peaks at 307 (red curve) and 410 nm (blue curve) due to π to π^* and n to π^* transitions in the carbon–oxygen, carbon–carbon, and molecular unsaturation centers.[24] The emission peak for NR-CDs was located at 420 nm under an excitation of 330 nm, as shown in curve b in Fig. 1A. The asymmetry and broad bands of NR-CDs reflect that their fluorescence could result from the functional groups on the carbon backbone combining with the localized sp^2 carbon subdomains.[25] The core state of NR-CDs refers to their interior structure, where carbon, nitrogen, and oxygen atoms are arranged in specific configurations.[26] In this core state, the sp^2 hybridized carbon atoms contribute to generating certain energy levels that can result in fluorescence. Additionally, the carboxylic acid, amino, and hydroxyl groups on the surface of NR-CDs introduce additional energy levels within the NR-CD energy band structure. The interaction of excitation energy with these surface functional groups can lead to modified emission properties. Furthermore, the NR-CDs had a relative quantum yield of 21%, as determined by comparison with standard quinine sulfate. This quantum yield is comparable to those reported for similar CDs derived from plants in a previous study.[27] To assess the stability of NR-CDs, we recorded their absorbance and fluorescence spectra during storage (Fig. 1B and S1, ESI†).

In Fig. 1C, the fluorescence spectra of the NR-CDs are presented for various excitation wavelengths ranging from 270 nm to 390 nm. The fluorescence intensity of NR-CDs showed a notable increase when excited between 270 nm and 330 nm. However, their fluorescence intensity gradually decreased beyond the excitation wavelength of 330 nm. When the excitation wavelength was adjusted to 330 nm, the highest intensity of emission peaks was observed at 420 nm. It's evident that the NR-CDs exhibited excitation-dependent emission behaviour, which is highly related to numerous functional groups on their surface.[28] This phenomenon may give rise to a collection of surface-state emissive traps capable of capturing and subsequently releasing energy, resulting in a broad and adjustable emission spectrum.[29] The emission color of the NR-CDs was assessed using the Commission Internationale de l'Eclairage (CIE) chromaticity coordinates, and emission data were recorded using Osram Sylvania software. Fig. 1D illustrates that the emission color corresponds to Fig. 1C, with CIE (X, Y) coordinates of (0.193, 0.176) for a maximum excitation wavelength of 330 nm.

This outcome underscores that the NR-CDs exhibit exceptional characteristics as UV-visible color converter materials. The blue emission color observed in NR-CDs aligns closely with the chromaticity coordinate diagram, emphasizing their potential value in applications related to color conversion and display technologies.[30] FT-IR, XRD, and TEM characterized the

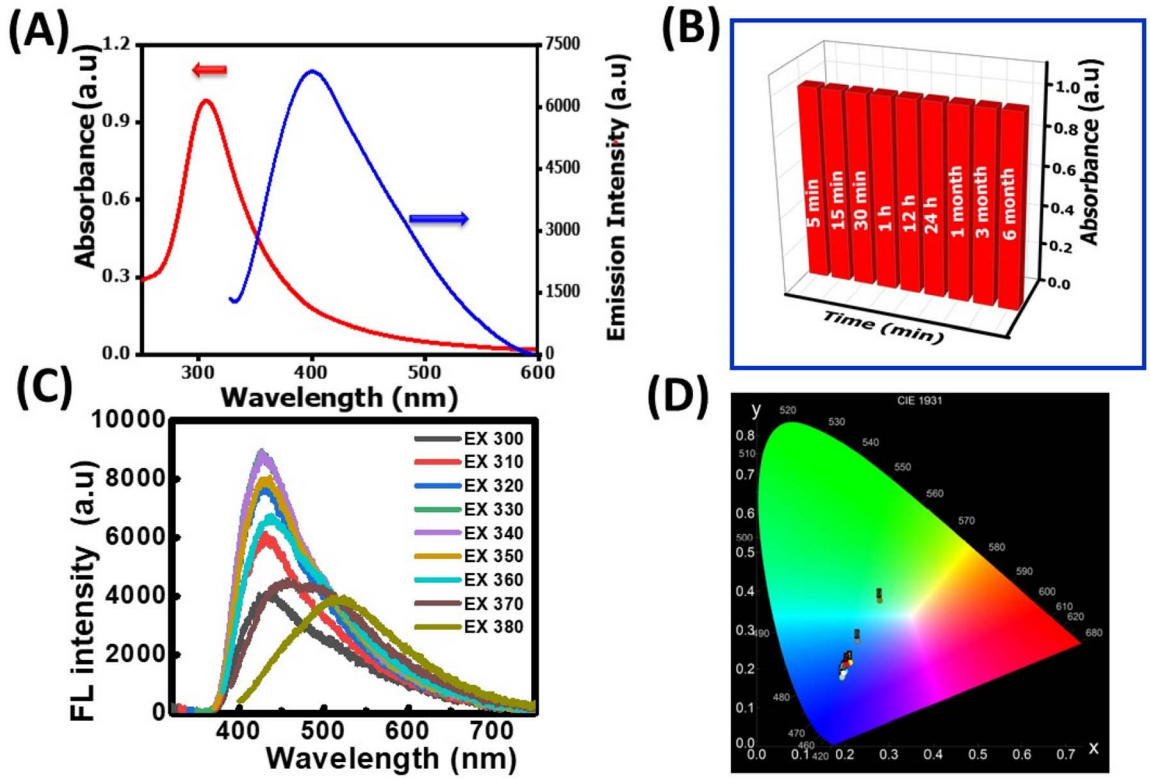

Fig. 1 Spectroscopic and photophysical properties of NR-CDs. (A) UV-vis absorption spectrum (red curve) and fluorescence spectrum (blue curve) of NR-CDs at an emission wavelength of 420 nm. (B) Time-dependent fluorescence intensity of the NR-CD probe. (C) Excitation-dependent emission spectra of NR-CDs with varying excitation wavelengths ranging from 270 to 390 nm. (D) Chromaticity coordinate diagram of NR-CDs.

chemical composition and morphology of the NR-CDs. Fig. 2A shows the FT-IR spectra of NR-CDs and neem resin extracts, indicating that the peaks observed at 3361 and 2086 cm^{-1} belong to the O–H (hydroxyl) and N–H stretching vibrations, respectively.[31] The 1643, 1064, and 662 cm^{-1} peaks were also identified as the –C═C, C–O–C, and C–OH in sequence.[31] These results confirm the presence of hydroxyl, carbonyl, and amine functional groups bound to the surface of NR-CDs. The XRD analysis is performed to determine the crystalline structure of NR-CDs. The XRD diffraction pattern of NR-CDs reveals a distinct strong Bragg reflection at 22.9° and 43°, corresponding to the (002) and (100) planes of graphitic carbon,[32] respectively (Fig. 2B). The XRD diffractogram of NR-CDs closely matched with the conventional powder diffraction reference (JCPDS26-1076) for graphitic carbon.[33]

Moreover, these broad and diffuse diffraction peaks suggest an amorphous nature of NR-CDs.[34] The TEM images showed that the NR-CDs were well dispersed and spherical, with a particle size of about 4.0 ± 0.2 nm (Fig. 2C); in the high magnification, it's clear that the as developed NR-CDs were composed of graphitic layers[19] with an interlayer spacing of 0.21 nm (Fig. 2D). This comprehensive characterization underscores the unique structural and chemical properties of NR-CDs, making them promising candidates for various applications.[35]

3.2. Fluorescent sensing of Fe^{2+} with the NR-CDs

Determining Fe^{2+} levels is crucial for maintaining optimal health due to its involvement in iron absorption, hemoglobin synthesis, oxygen transport, energy production, and enzymatic functions.[36] Regularly monitoring Fe^{2+} levels allows healthcare professionals to identify and address deficiencies or abnormalities, such as anemia and Alzheimer's. Beyond the physiological role, iron concentration imbalances in soil and water can harm the environment.[37] Therefore, the rapid and reliable detection of Fe^{2+} ions in biological and environmental samples is paramount.

The TEM image shows that incubation with Fe^{2+} ions could induce the aggregation of NR-CDs (Fig. 2E), which inspired us to explore further, and the size of the aggregated NR-CDs was estimated to be 28.7 ± 0.2 nm. As shown in Fig. 3A and B the prominent absorption peak of NR-CDs at 307 nm and their fluorescence peak at 420 nm gradually reduced as the concentration of Fe^{2+} ions varied from 0 to 61 μM.[38] Plotting the fluorescence intensity at 420 nm against the concentration of Fe^{2+} ions resulted in a linear calibration curve ($R^2 = 0.9934$, Fig. 3C) in the range of 4 to 71 μM.[39] The limit of detection (LOD) for Fe^{2+} ions was determined to be 14 nM (signal-to-noise ratio of 3) using this proposed NR-CD fluorescence probe; generally this LOD can be calculated by using the $3\sigma/m$ formula, where "σ" is the standard deviation and "m" is the slope of the calibration

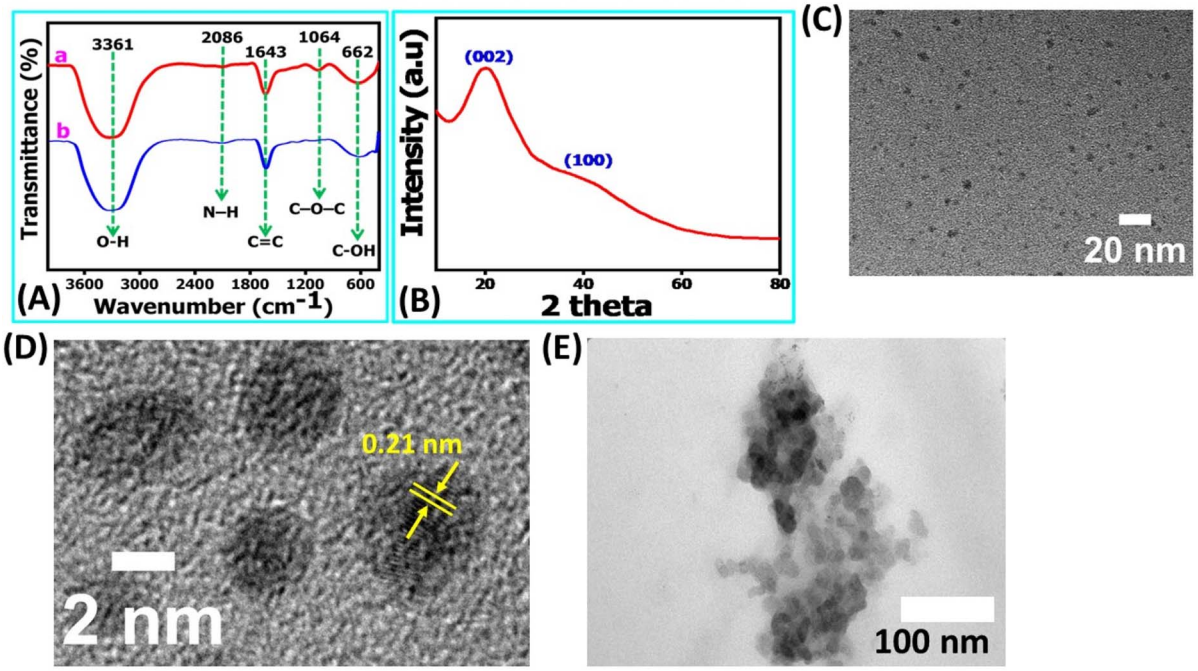

Fig. 2 Characterization and morphological analysis of NR-CDs and their interaction with Fe^{2+} ions. (A) FT-IR spectra of neem resign extracts (dark red line) and the NR-CDs (dark blue line). (B) XRD pattern and (C and D) TEM image of the NR-CDs. (E) TEM image of NR-CDs in the presence of 62 μM of Fe^{2+} ions.

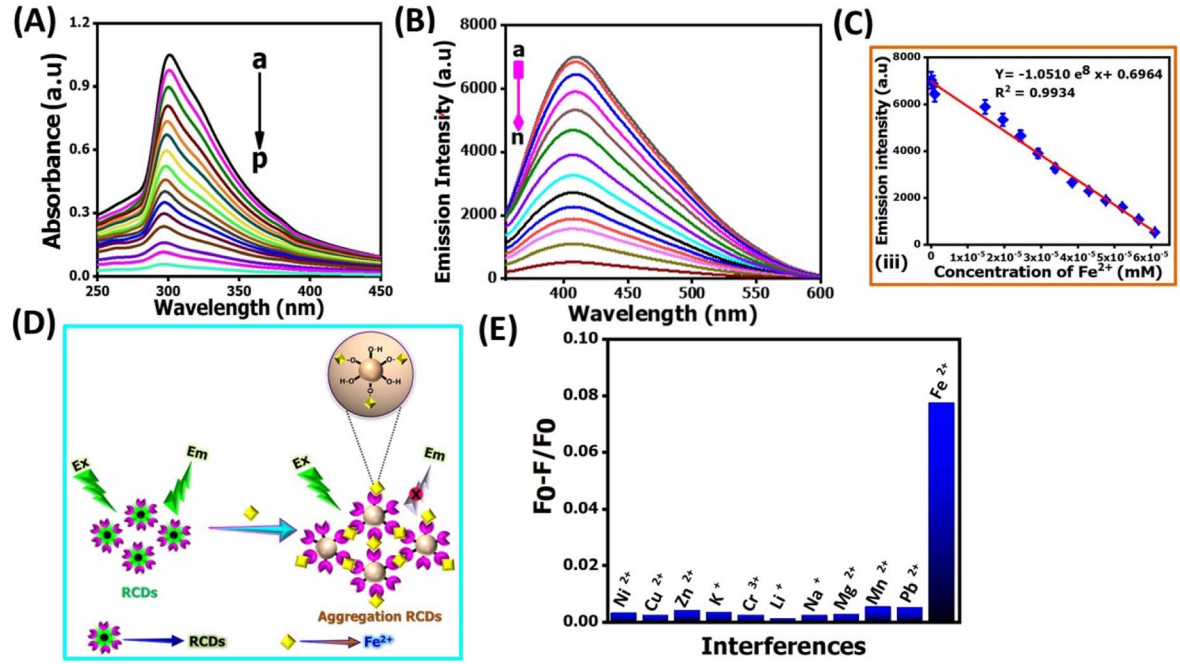

Fig. 3 Spectroscopic characterization and sensing mechanism of NR-CDs for Fe^{2+} ions. (A) UV-vis absorption and (B) fluorescence spectra obtained from the incubation of NR-CDs with different concentrations of Fe^{2+} ions at pH 7.2. The arrow represents variations in absorbance and fluorescence intensity with increasing Fe^{2+} ion concentration. (A) The concentrations studied were as follows: (a) blank, (b) 4, (c) 9, (d) 14, (e) 19, (f) 23, (g) 28, (h) 33, (i) 38, (j) 42, (k) 47, (l) 51, (m) 57, (n) 61, (o) 65, and (p) 71 μM. (B) The concentrations studied were as follows: (a) blank, (b) 4, (c) 9, (d) 14, (e) 19, (f) 23, (g) 28, (h) 33, (i) 38, (j) 42, (k) 47, (l) 51, (m) 57 and (n) 61 μM. (C) The excitation wavelength was set to 330 nm, a photograph of NR-CDs before and after adding 62 μM Fe^{2+} ions. A calibration graph illustrating the relationship between fluorescence intensity at 420 nm and the concentration of Fe^{2+} ions. (D) Schematic illustration for the sensing mechanism of NR-CDs for Fe^{2+} ions. (E) The $(F_0 - F)/F$ value and photographs obtained from the incubation of NR-CDs with Fe^{2+} ions (62 μM) and other metal ions (4.8 mM). From left to right, the tested ions included Ni^{2+}, Cu^{2+}, Zn^{2+}, K^{+}, Cr^{3+}, Li^{+}, Na^{+}, Mg^{2+}, Mn^{2+}, Pb^{2+}, and Fe^{2+} ions.

Table 1 Comparison of NR-CDs with previous reports

S. no	Probe	Synthesis method	Quantum yield (%)	LOD (nM)	Real sample	Ref.
1	Cornstalk derived C-Dots	Hydrothermal	7.6	180	No reaction	38
2	Polyetherimide and N,N,2-methylformamide	Hydrothermal	No reaction	160	Tap water	39
3	Amino trimethylene phosphonic acid and trisodium citrate	Hydrothermal	17.74	298	River water and tap water	40
4	Ascorbic acid and thioglycolic acid	Hydrothermal	32.07	50	Oral ferrous gluconate	41
5	Acrylamide/chitosan	Microwave-hydrothermal	12.17	160	Drinking water	42
6	Citric acid and 1,10-phenanthroline	Hydrothermal	10	20	Milk	43
7	Glutathione capped GQDs	Pyrolysis	No reaction	100	Drinking water	44
8	M-aminobenzoic acid	Hydrothermal	30.7	50	Lake water	45
9	Aspartic acid and NH_4HCO_3	Microwave irradiation	14	260	No reaction	46
10	NR-CDs	Hydrothermal	21	14	Tap water, river water and drinking water	This work

graph and 3 is three times replication. This LOD value is lower than that from previously reported similar CDs, derived from plants in earlier studies,[38–46] as shown in Table 1.

These findings reflect that Fe^{2+} ions could complex with the functional groups on the surface of NR-CDs, triggering their aggregation.[43] The as-formed aggregates can scatter incident light, reducing the absorbance and fluorescence intensity of NR-CDs (Fig. 3D). Next, we examined the selectivity of NR-CDs toward Fe^{2+} in the presence of possible interfering metal ions.[44] The fluorescence intensity of NR-CDs in the absence and presence of metal ions was denoted as F_0 and F. Thus, the value of $(F_0 - F)/F$ can be used to evaluate the effect of metal ions on the selectivity of NR-CDs. Fig. 3E shows that only Fe^{2+} ions at a concentration of 62 μM induced a significant increase in the $(F_0 - F)/F$ value.[45] In contrast, other metal ions at 4.8 mM had a minimal impact on the $(F_0 - F)/F$ value.

This result suggests that the selectivity of NR-CDs for Fe^{2+} exceeds a 100-fold difference compared to the other metal ions. In our study, we gathered genuine water samples of diverse origins, encompassing river, tap, and drinking water, after subjecting them to a straightforward filtration process. Subsequently, we spiked 10 μM and 20 μM of Fe^{2+} ions into these samples and subjected them to analysis by using NR-CDs. The outcome of these experiments was remarkable, with recovery

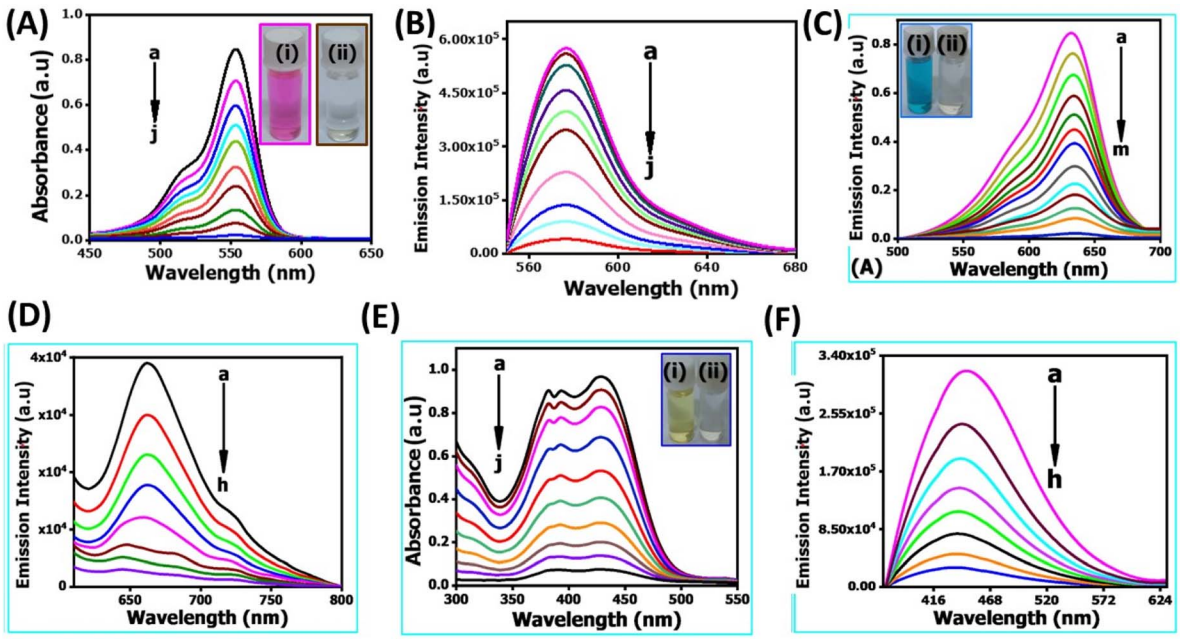

Fig. 4 Photocatalytic degradation of Rhodamine B, Fast Green, and Naphthol Yellow with NR-CDs. Time-dependent (A, C, and E) UV-vis and (B, D and F) fluorescence spectra obtained from the incubation of (A and B) 100 mM of Rhodamine B, (C and D) 100 mM of Fast Green, and (E and F) 100 mM of Naphthol Yellow with 5 mM $NaBH_4$ and the NR-CDs under the exposure of visible light (456 nm). The reaction times span from (A and B) a to j, (C) a to m, (D) a to h, (E) a to j, and (F) a to h with a 1 min interval. Photographic images of (A) Rhodamine B, (C) Fast Green, and (E) Naphthol Yellow (i) before and (ii) after photocatalytic degradation treatment.

Table 2 Determination of Fe^{2+} ions in different real samples using NR-CDs

S. no	Sample	Fe^{2+} ions spiked (μM)	Fe^{2+} ions found (μM)	Recovery (%)	SD	RSD
1	Tap water	—	0	—	—	—
		10	9.7	97	1.5	1.63
		20	19.2	96	1.7	1.77
2	River water	—	0	—	—	—
		10	9.8	98	2.4	2.5
		20	19.7	98.5	1.0	1.02
3	Drinking water	—	0	—	—	—
		10	9.7	97	0.9	0.94
		20	19.7	98.5	0.7	0.78

rates falling within the range of 95% to 98.5%. These findings underscore the robustness and reliability of the NR-CD assay for the detection of Fe^{2+} ions in various water sources as shown in Table 2.[46]

3.3. Photocatalytic degradation of Rhodamine B dye

In recent years, the degradation of organic dyes has become a crucial area of research due to the increasing concern over water pollution and the need for effective wastewater treatment methods.[47] Nanomaterials, with their unique properties and high surface area,[48] have emerged as promising candidates for the degradation of organic dyes.[49,50] In comparison to other nanomaterials, the NR-CDs have gained significant interest in the field of environmental remediation, particularly for the degradation of organic dyes.[51] The primary advantages of carbon dots (CDs) over other nanomaterials stem from their broad absorption spectrum, which spans from ultraviolet (UV) to the visible light range. This extensive absorption capability enables efficient energy transfer and the absorption of photons across a wide range of wavelengths.[52] Additionally, their small size and large surface area provide more active sites for chemical reactions, enhancing their catalytic efficiency.[53] Leveraging these advantages, we degraded three organic dyes in the presence of NR-CDs serving as the catalyst, with $NaBH_4$ as a surface defect modifier and UV light as the driving energy source.[52] This combined approach capitalizes on the unique properties of NR-CDs to facilitate the efficient degradation of organic dyes, making NR-CDs a promising system for photocatalytic applications. Fig. 4A and B show that the absorbance and fluorescence intensity of Rhodamine B exhibited a gradual reduction with the extension of reaction time when exposed to $NaBH_4$ under visible light.[53] Under an identical treatment, similar phenomena were observed in green dye (Fig. 4C and D) and Naphthol Yellow (Fig. 4E and F); the NR-CD mediated photodegradation of Rhodamine B, Fast Green, and Naphthol Yellow was almost completed within 9, 12, and 7 min, respectively, in the presence of $NaBH_4$. By contrast, the short-time complete degradation of these three organic dyes was rarely achieved without addition of NR-CDs, $NaBH_4$, or visible light. The photographs of the three organic dyes before and after the introduction of NR-CDs, $NaBH_4$, and visible light could help visualize the success of the photocatalytic degradation,[53] showing the transformation of dyes from their pristine state to a colourless state under the catalyst and visible light irradiation (insets in Fig. 4A, C, and E).

Upon degrading a mixture of three organic dyes, we observed a significant decrease in the absorption and fluorescence peaks associated with these dyes in only 8 min (Fig. 5A and B). It has been demonstrated that the NR-CDs, combined with $NaBH_4$ and under the influence of visible light, can simultaneously promote the degradation of several organic dyes. This observation is crucial for efficiently removing complex dye mixtures in wastewater treatment and environmental remediation processes.[54] The degradation efficiency of these three organic dyes was assessed by continuously monitoring the maximum absorbance intensity at various time intervals while maintaining the concentration of the organic dyes and $NaBH_4$ constant.[54] The degradation efficiency can be determined according to the following eqn (1):

$$\text{degradation efficiency}(\%) = \frac{C_0 - C_t}{C_0} \times 100\% \quad (1)$$

where C_0 represents the initial concentration of the dye, and C_t stands for the concentration of the dye at a specific irradiation time (t).[48] The degradation efficiency of Rhodamine B, Fast Green, and Naphthol Yellow dye demonstrated a notable improvement as the reaction time was extended (Fig. 5C). This increased degradation efficiency signifies the effectiveness of the photocatalytic process using the NR-CDs and $NaBH_4$, particularly in the progressive degradation of the organic dyes over time.[55] Under these conditions, the degradation efficiency of the proposed catalytic system for Rhodamine B, Fast Green, and Naphthol Yellow was determined to be 93.13%, 93.01%, and 91.29%, respectively. The reaction kinetics of the three different organic dyes can be elucidated by employing their pseudo-first-order kinetics (eqn (2)):[48]

$$\ln\frac{F_t}{F_0} = K_t \quad (2)$$

where F_t, F_0 and K_t are the initial absorbance intensity of the organic dye, the time-evolved absorbance intensity of the organic dye, and reaction time, respectively. Fig. 5D shows a good linear relationship between the natural logarithm of F_t/F_0 and reaction time.[55] The rate constants of the proposed catalytic system for Rhodamine B, Fast Green, and Naphthol Yellow dye were calculated to be 0.2707, 0.1262, and 0.2917 min^{-1} in sequence. As shown in Fig. S2, ESI†, the band gap energies of the NR-CD nano-catalyst, estimated by the Kubelka–Munk function were calculated to be 2.87 eV, signifying that the NR-CD nano-catalyst can enhance the visible light absorption ability to promote the catalytic degradation of various organic dyes such as Rhodamine B, Fast Green, and Naphthol Yellow. To support our phenomena, we further conducted electron paramagnetic resonance spectroscopy (EPR),[56] which is a powerful tool for identifying the types of radicals present in radical-related photocatalytic reactions; because of the short half-life of radicals, their direct detection is infeasible by EPR.[56] Luckily, radicals can be captured by reacting with spin trapping agents, such as 2,2,6,6-tetramethylpiperidine and 5,5-

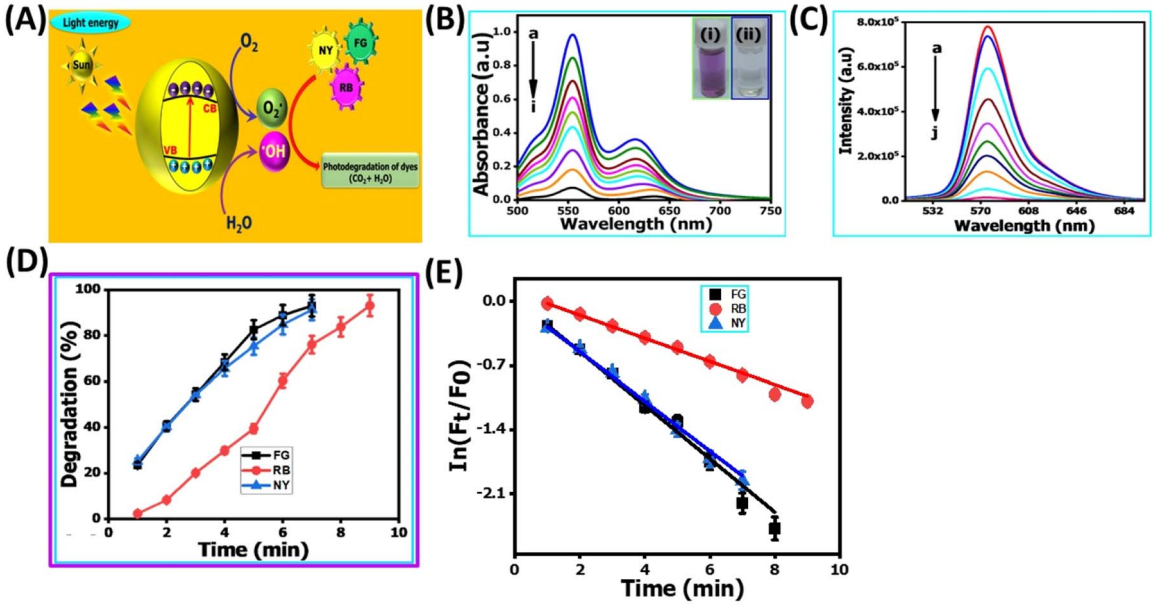

Fig. 5 (A) Schematic illustration for the proposed photocatalytic degradation mechanism which involves the NR-CDs, $NaBH_4$, and organic dyes under visible light, (B) UV-vis spectra and (C) fluorescence spectra obtained from the incubation combination of 100 mM of Rhodamine B, 100 mM of Fast Green, and 100 mM of Naphthol Yellow with 100 μl of $NaBH_4$ (5 mM) and 1000 μl of NR-CDs under the exposure of visible light (456 nm). (D) The degradation efficiency of 100 mM of Rhodamine B (red line), 100 mM of Fast Green (black line), and 100 mM of Naphthol Yellow (blue line) at various reaction times. (E) A linear relationship between the natural logarithm of F_t/F_0 and reaction time for Rhodamine B (red line), Fast Green (black line), and Naphthol Yellow (blue line).

dimethyl-1-pyrroline-*N*-oxide (DMPO), to form stable spin-adducts.[56] After mixing the NR-CD nano-catalyst with DMPO in the presence of dissolved O_2 for 30 min, no EPR signal was observed without the irradiation of visible light (curve blue line in Fig. S2B, ESI†). Under the same reaction conditions, the presence of visible light produced a four-line hyperfine splitting with 1 : 2 : 2 : 1 intensity ratio in the EPR spectra (curve red line in Fig. S2B, ESI†), signifying the formation of DMPO-OH adducts. In alongside we were established conducting their mechanism of photo-catalytic degradation for various organic dyes were strongly believe that, the fluorescence spectroscopy for monitoring the oxidation of terephthalic acid into 2-hydroxyterephthalic acid in the presence of our proposed catalyst of the NR-CD nano-catalyst as shown in Fig. S3, ESI†. Based on the above studies, we concluded that the OH˙ could be mainly responsible for the degradation of various organic dyes, and recent literature studies also support our proposed mechanism. Next, we propose a possible mechanism for the catalytic system under the following pathways (Fig. 5E): (1) when exposed to visible light, the NR-CDs absorb photons, creating electron–hole pairs within the NR-CD structure. (2) $NaBH_4$ functions as a reducing agent to form more surface defects on the NR-CD surface, generating more active sites.[52] (3) Organic dyes, including Rhodamine B, green dye, and Naphthol yellow, are drawn to the surface of NR-CDs due to van der Waals interactions and electrostatic forces. These dyes become adsorbed onto the NR-CD surface. (4) Some of the electrons (e^-) are captured due to the surface defects, delaying the recombination of electron (e^-) and photon (h^+) couples, and others are captured by dissolved oxygen, producing superoxide radicals ($^{\bullet}O_2^-$). (5) The three dyes are degraded in the presence of ($^{\bullet}O_2^-$) highly active oxygen.[56] The photosensitized photons (h^+) directly interact with dye molecules to produce organic radicals or combine with surface-adsorbed water molecules to produce hydroxyl radicals ($^{\bullet}OH$). Reactive oxygen species interact with the dye molecules and influence the degradation of the three dye molecules concurrently.[56]

4. Conclusion

The NR-CDs were successfully synthesized through an environmentally friendly approach, avoiding organic solvents. The NR-CDs had a high quantum yield of 21% and exhibited stable fluorescence over time. The comprehensive characterization of NR-CDs demonstrates their unique structural and optical properties, positioning them as a promising candidate for sensing Fe^{2+} ions and photodegradation of organic dyes. We have successfully employed the NR-CDs as a reliable tool for probing Fe^{2+} ions. The NR-CD probe offered a low limit of detection (14 nM) and exceptional selectivity, with a 100-fold difference compared to other interfering metal ions. Furthermore, our experiments on real water samples demonstrated the practicality of the NR-CD assay, yielding an impressive recovery rate ranging from 95% to 98.5%. These results affirm the effectiveness and versatility of NR-CDs for accurately detecting Fe^{2+} ions in diverse water sources. The photocatalytic degradation of organic dyes by using NR-CDs and $NaBH_4$ under visible light has been demonstrated as an effective and promising approach. The proposed mechanism suggests a multi-step

process involving electron–hole pair generation, surface defect modification using $NaBH_4$, adsorption of organic dyes, the capture of electrons by surface defects and superoxide radicals, and degradation of dye molecules through the interaction of reactive oxygen species. It is suggested that NR-CDs have the capacity to absorb and convert a wide range of light (visible region), promising to be a suitable candidate for solar energy conversion.

Data availability

The data that support the findings of this study are available from the corresponding author upon reasonable request. All relevant codes are available in the ESI† or from the corresponding author on request.

Author contributions

S. Gokul Eswaran: conceptualization, methodology, formal analysis, data curation, writing – original draft. T. Stalin: investigation. D. Thiruppathi: data curation [(Jolanta Warchol, Santhoshkumar, writing – review & editing)]. Manivannan Madhu: formal analysis, investigation, writing – review & editing. A. Santhana Krishna Kumar: conceptualization, methodology, data curation, investigation, writing – review & editing. Wei-Lung Tseng: investigation, writing – review & editing. Nagamalai Vasimalai: conceptualization, writing – review & editing, resources, funding acquisition. All authors discussed the results and commented on the manuscript.

Conflicts of interest

The authors declare no competing interests.

Acknowledgements

S. Gokul Eswaran thanks B. S. Abdur Rahman Crescent Institute of Science and Technology, Chennai-600 048, India for the award of Junior Research Fellow under the BSA-JRF University Fellowship (Lr. No. 773/Dean (R) 2019/05.08.2019).

References

1 S. Ahmed and M. Grainge, Potential of the neem tree (Azadirachta indica) for pest control and rural development, *Econ. Bot.*, 1986, **40**, 201–209.
2 J. F. Islas, E. Acosta, Z. G-Buentello, J. L. Delgado-Gallegos, M. G. Moreno-Treviño, B. Escalante and J. E. Moreno-Cuevas, An overview of neem (*Azadirachta indica*) and its potential impact on health, *J. Funct. Foods*, 2020, **74**, 104171.
3 S. C. Gupta, S. Prasad, A. K. Tyagi, A. B. Kunnumakkara and B. B. Aggarwal, Neem (*Azadirachta indica*): An indian traditional panacea with modern molecular basis, *Phytomedicine*, 2017, **34**, 14–20.
4 A. Verma and M. S. Mehata, Controllable synthesis of silver nanoparticles using Neem leaves and their antimicrobial activity, *J. Radiat. Res. Appl. Sci.*, 2016, **9**, 109–115.
5 A. Tripathy, A. M. Raichur, N. Chandrasekaran, T. C. Prathna and A. Mukherjee, Process variables in biomimetic synthesis of silver nanoparticles by aqueous extract of *Azadirachta indica* (Neem) leaves, *J. Nanopart. Res.*, 2010, **12**, 237–246.
6 A. Tripathi, N. Chandrasekaran, A. M. Raichur and A. Mukherjee, Antibacterial applications of silver nanoparticles synthesized by aqueous extract of *Azadirachta Indica* (Neem) leaves, *J. Biomed. Nanotechnol.*, 2009, **5**(1), 93–98.
7 N. Namratha and P. V. Monica, Synthesis of silver nanoparticles using *Azadirachta indica* (Neem) extract and usage in water purification, *Asian J. Pharm. Technol.*, 2013, **3**(4), 170–174.
8 K. Chand, M. Ishaque Abro, U. Aftab, A. Hussain Shah, M. Nazim Lakhan, D.-X. Cao, G. Mehdi and A. M. Ali Mohamed, Green synthesis characterization and antimicrobial activity against *Staphylococcus aureus* of silver nanoparticles using extracts of neem, onion and tomato, *RSC Adv.*, 2019, **9**, 17002–17015.
9 S. S. Shankar, A. Rai, A. Ahmad and M. Sastry, Rapid synthesis of Au, Ag and bimetallic Au core Ag shell nanoparticles using neem (*Azadirachta indica*) leaf broth, *J. Colloid Interface Sci.*, 2004, **275**(2), 496–502.
10 C. M. Noorjahan, Sk. Jasmine Shahina, D. Thangaraj and S. Rafiq, Green synthesis and characterization of zinc oxide nanoparticles from neem (*Azadirachta indicia*), *Int. J. Eng. Sci. Technol.*, 2015, **4**(30), 5751–5753.
11 S. A. Korde, P. B. Thombre, S. S. Dipake, J. N. Sangshetti, A. S. Rajbhoj and S. T. Gaikwad, Neem gum (*Azadirachta indicia*) facilitated green synthesis of TiO_2 and ZrO_2 nanoparticles as antimicrobial agents, *Inorg. Chem. Commun.*, 2023, **153**, 110777.
12 M. Pattanayak and P. L. Nayak, Green synthesis and characterization of zero valent iron nanoparticles from the leaf extract of *Azadirachta indica* (Neem), *World J. Nano Sci. Eng.*, 2013, **2**(1), 06–09.
13 S. Krishna Moorthy, C. H. Ashok, K. Venkateswara Rao and C. Viswanathan, Synthesis and characterization of MgO nanoparticles by neem leaves through green method, *Mater. Today: Proc.*, 2015, **2**(9), 4360–4368.
14 N. D. Syazwani Zambri, N. I. Taib, F. Abdul Latif and Z. Mohamed, Utilization of neem leaf extract on biosynthesis of iron oxide nanoparticles, *Molecules*, 2019, **24**(20), 3803.
15 M. Mahara and Y. Singh, Tribological analysis of the neem oil during the addition of SiO_2 nanoparticles at different loads, *Mater. Today: Proc.*, 2020, **28**, 1412–1415.
16 V. Gopalakrishnan and S. Muniraj, Neem flower extract assisted green synthesis of copper nanoparticles optimization, characterization and anti-bacterial study, *Mater. Today: Proc.*, 2021, **36**(4), 832–836.
17 N. Javed and D. M. O'Carroll, Carbon dots and stability of their optical properties, *Part. Part. Syst. Charact.*, 2021, **38**(4), 2000271.
18 V. Magesh, A. K. Sundramoorthy and D. Ganapathy, Recent advances on synthesis and potential applications of carbon quantum dots, *Front. Mater.*, 2022, **9**, 906838.

19 S. C. Kishore, S. Perumal, R. Atchudan, T. N. J. Immanuel Edison, A. K. Sundramoorthy, M. Alagan, S. Sangaraju and Y. R. Lee, Eco-friendly synthesis of functionalized carbon nanodots from cashew nut skin waste for bioimaging, *Catalysts*, 2023, **13**, 547.

20 R. Atchudan, S. Perumal, T. N. J. I. Edison, A. K. Sundramoorthy, R. Vinodh, S. Sangaraju, S. C. Kishore and Y.-R. Lee, Natural nitrogen-doped carbon dots obtained from hydrothermal carbonization of chebulic myrobalan and their sensing ability toward heavy metal ions, *Sensors*, 2023, **23**, 787.

21 S. M. Selvan, K. V. Anand, V. Magesh, A. K. Sundramoorthy, G. Vinitha, A. Khosla and K. Govindaraju, Green synthesis of blue light-emitting carbon dots using tridax procumbens leaves: Optical and electrochemical studies, *ECS J. Solid State Sci. Technol.*, 2023, **12**, 067007.

22 X. Lin, M. Xiong, J. Zhang, H. Chen, X. Ma, H. Zhang, Y. Kuang, M. Yang and Q. Huang, Carbon dots based on natural resources: Synthesis and applications in sensors, *Microchem. J.*, 2021, **160**, 105604.

23 J. Lim, M. Choi, H. J. Lee, Y.-Ho Kim, Ji-Y. Han, E. S. Lee and Y. Cho, Direct isolation and characterization of circulating exosomes from biological samples using magnetic nanowires, *J. Nanobiotechnol.*, 2019, **17**(1), 1–24.

24 S. Thiyagarajan, S. Raghupathy, D. Palanivel, K. Raji and P. Ramamurthy, Fluorescent carbon nano dots from lignite: unveiling the impeccable evidence for quantum confinement, *Phys. Chem. Chem. Phys.*, 2016, **18**, 12065–12073.

25 H. Liu, T. Ye and C. Mao, Fluorescent carbon nanoparticles derived from candle soot, *Angew. Chem., Int. Ed.*, 2007, **119**, 6593–6595.

26 X. Wen, P. Yu, Y.-R. Toh, X. Hao and J. Tang, Intrinsic and extrinsic fluorescence in carbon nanodots: Ultrafast time-resolved fluorescence and carrier dynamics, *Adv. Opt. Mater.*, 2013, **1**, 173–178.

27 M. Zulfajri, H. N. Abdelhamid, S. Sudewi, S. Dayalan, A. Rasool, A. Habib and G. G. Huang, Plant part-derived carbon dots for biosensing, *Biosensors*, 2020, **10**(6), 68.

28 M. Madhu, T.-H. Chen and W.-L. Tseng, White-light emission of single carbon dots prepared by hydrothermal carbonization of poly(diallyldimethylammonium chloride): Applications to fabrication of white-light-emitting films, *J. Colloid Interface Sci.*, 2019, **556**(15), 120–127.

29 X. Li, S. Zhang, S. A. Kulinich, Y. Liu and H. Zeng, Engineering surface states of carbon dots to achieve controllable luminescence for solid-luminescent composites and sensitive Be^{2+} detection, *Sci. Rep.*, 2014, **4**, 4976.

30 H.-Y. Lin, C.-C. Liao and M.-Y. Hua, Fabrication of zinc protoporphyrin-modified gold electrode for sensitive and fast detection of vascular endothelial growth factor, *Chemosensors*, 2021, **9**, 21.

31 Y. Liu, X. Shen, H. Zhou, Y. Wang and L. Deng, Chemical modification of chitosan film *via* surface grafting of citric acid molecular to promote the biomineralization, *Appl. Surf. Sci.*, 2016, **370**, 270–278.

32 E. Arputharaj, A. Santhana Krishna Kumar, W. L. Tseng, S. J. Jiang, Y. L. Huang and H.-U. Dahms, Self-Assembly of poly(ethyleneimine)-modified g-C_3N_4 Nanosheets with lysozyme fibrils for chromium detoxification, *Langmuir*, 2021, **37**, 7147–7155.

33 R. Md Salim, J. Asik and M. S. Sarjadi, Chemical functional groups of extractives, cellulose and lignin extracted from native *Leucaena leucocephala* bark, *Wood Sci. Technol.*, 2021, **55**, 295–313.

34 Y. Osuna, K. M. Gregorio-Jauregui, J. G. Gaona-Lozano, I. M. de la Garza-Rodriguez, A. Ilyna, E. D. Barriga-Castro, H. Saade and R. G. Lopez, Chitosan-coated magnetic nanoparticles with low chitosan content prepared in one-step, *J. Nanomater.*, 2012, **2012**, 1–7.

35 M. Zaib, A. Akhtar, F. Maqsood and T. Shahzadi, Green synthesis of carbon dots and their application as photocatalyst in dye degradation studies, *Arabian J. Sci. Eng.*, 2021, **46**, 437–446.

36 N. Abbaspour, R. Hurrell and R. Kelishadi, Review on iron and its importance for human health, *J. Res. Med. Sci.*, 2014, **19**(2), 164–174.

37 G. R. Rout and S. Sahoo, Role of iron in plant growth and metabolism, *Rev. Agric. Sci.*, 2015, **3**, 1–24.

38 J. Shi, G. Ni, J. Tu, X. Jin and J. Peng, Green synthesis of fluorescent carbon dots for sensitive detection of Fe^{2+} and hydrogen peroxide, *J. Nanopart. Res.*, 2017, **19**, 209.

39 S. Wei, L. Tan, X. Yin, R. Wang, X. Shan, Q. Chen, T. Li, X. Zhang, C. Jiang and G. Sun, A sensitive "ON–OFF" fluorescent probe based on carbon dots for Fe^{2+} detection and cell imaging, *Analyst*, 2020, **145**, 2357–2366.

40 S.-R. Zhang, S.-K. Cai, G.-Q. Wang, J.-Z. Cui and C.-Z. Gao, One-step synthesis of N, P-doped carbon quantum dots for selective and sensitive detection of Fe^{2+} and Fe^{3+} and scale inhibition, *J. Mol. Struct.*, 2021, **1246**, 131173.

41 F. Du, Z. Cheng, W. Tan, L. Sun and G. Ruan, Development of sulfur doped carbon quantum dots for highly selective and sensitive fluorescent detection of Fe^{2+} and Fe^{3+} ions in oral ferrous gluconate samples, *Spectrochim. Acta, Part A*, 2020, **226**, 117602.

42 G. Liu, B. Li, Y. Liu, Y. Feng, D. Jia and Y. Zhou, Rapid and high yield synthesis of carbon dots with chelating ability derived from acrylamide/chitosan for selective detection of ferrous ions, *Appl. Surf. Sci.*, 2019, **487**, 1167–1175.

43 M. Iqbal, A. Saeed and S. I. Zafar, FT-IR spectrophotometry, kinetics and adsorption isotherms modeling, ion exchange, and EDX analysis for understanding the mechanism of Cd^{2+} and Pb^{2+} removal by mango peel waste, *J. Hazard. Mater.*, 2009, **164**, 161–171.

44 K. Saenwong, P. Nuengmatcha, P. Sricharoen, N. Limchoowong and S. Chanthai, GSH-doped GQDs using citric acid rich-lime oil extract for highly selective and sensitive determination and discrimination of Fe^{3+} and Fe^{2+} in the presence of H_2O_2 by a fluorescence "turn-off" sensor, *RSC Adv.*, 2018, **8**, 10148–10157.

45 R. Wang, X. Wang and Y. Sun, One-step synthesis of self-doped carbon dots with highly photoluminescence as

multifunctional biosensors for detection of iron ions and pH, *Sens. Actuators, B*, 2017, **241**, 73–79.

46 C. Zhang, Y. Cui, L. Song, X. Liu and Z. Hu, Microwave assisted one-pot synthesis of graphene quantum dots as highly sensitive fluorescent probes for detection of iron ions and pH value, *Talanta*, 2016, **150**, 54–60.

47 A. Santhana Krishna Kumar, J. Warchol, J. Matusik, W.-L. Tseng, N. Rajesh and T. Bajda, Heavy metal and organic dye removal *via* a hybrid porous hexagonal boron nitride-based magnetic aerogel, *npj Clean Water*, 2022, **5**, 1–12.

48 A. Santhana Krishna Kumar, C.-Y. Lu and W.-L. Tseng, Two in one: Poly(ethyleneimine)-modified MnO_2 nanosheets for ultrasensitive detection and catalytic reduction of 2,4,6-Trinitrotoluene and other nitro aromatics, *ACS Sustain. Chem. Eng.*, 2021, **9**, 1142–1151.

49 E. Murugan, S. S. Kumar, K. M. Reshna and S. Govindaraju, Highly sensitive, stable g-CN decorated with AgNPs for SERS sensing of toluidine blue and catalytic reduction of crystal violet, *J. Mater. Sci.*, 2019, **54**(7), 5294–5310.

50 S. P. Ratnayake, M. Mantilaka, C. Sandaruwan, D. Dahanayake, E. Murugan, S. Santhosh Kumar, G. A. J. Amaratunga and K. M. Nalin de Silva, Carbon quantum dots-decorated nano-zirconia: A highly efficient photocatalyst, *Appl. Catal., A*, 2019, **570**, 23–30.

51 Y. Zhou, E. M. Zahran, B. A. Quiroga, J. Perez, K. J. Mintz, Z. Peng, P. Y. Liyanage, R. R. Pandey, C. C. Chusuei and R. M. Leblanc, Size-dependent photocatalytic activity of carbon dots with surface-state determined photoluminescence, *Appl. Catal., B*, 2019, **248**, 157–166.

52 D. Saini, A. Kumari Garg, C. Dalal, S. Raj Anand, S. Kumar Sonkar, A. Kumar Sonker and G. Westman, Visible-light-promoted photocatalytic applications of carbon dots: A review, *ACS Appl. Nano Mater.*, 2022, **5**(3), 3087–3109.

53 H. Zheng, Q. Wang, Y. Long, H. Zhang, X. Huang and R. Zhu, Enhancing the luminescence of carbon dots with a reduction pathway, *Chem. Commun.*, 2011, **47**, 10650–10652.

54 M. Chandhru, S. Kutti Rani and N. Vasimalai, Reductive degradation of toxic six dyes in industrial wastewater using diaminobenzoic acid capped silver nanoparticles, *J. Environ. Chem. Eng.*, 2020, **8**, 104225.

55 M. Chandhru, P. Gunasekaran, M. Maruthupandi, R. Meenakshi, M. Sundar, A. N. Kalanthoden, N. Ahmad, M. R. Khan, A. Santhana Krishna Kumar, S. K. Rani and N. Vasimalai, Bio-fabricated silver nano-catalyst for photocatalytic degradation and organic transformation of toxic pollutants, *Next Mater.*, 2023, 100023.

56 A. Santhana Krishna Kumar, W.-B. Tseng, E. Arputharaj, P.-J. Huang, W.-L. Tseng and T. Bajda, Covalent organic framework nanosheets as an enhancer for light-responsive oxidase-like nanozymes: Multifunctional applications in colorimetric sensing, antibiotic degradation, and antibacterial agents, *ACS Sustain. Chem. Eng.*, 2023, **11**, 6956–6969.